

Original article

Hydraulic properties of 3D crossed rock fractures by considering anisotropic aperture distributions

Richeng Liu^{1,2*}, Yujing Jiang^{2,3}, Na Huang², Satoshi Sugimoto²

¹State Key Laboratory for Geomechanics and Deep Underground Engineering, China University of Mining and Technology, Xuzhou 221116, P. R. China

²School of Engineering, Nagasaki University, 1-14 Bunkyo-machi, 8528521 Nagasaki, Japan

³State Key Laboratory of Mining Disaster Prevention and Control Co-founded by Shandong Province and the Ministry of Science and Technology, Shandong University of Science and Technology, Qingdao 266510, P. R. China

(Received February 15, 2018; revised March 2, 2018; accepted March 3, 2018; available online March 9, 2018)

Citation:

Liu, R., Jiang, Y., Huang, N., Sugimoto, S. Hydraulic properties of 3D crossed rock fractures by considering anisotropic aperture distributions. *Advances in Geo-Energy Research*, 2018, 2(2): 113-121, doi: 10.26804/ager.2018.02.01.

Corresponding author:

*E-mail: liuricheng@cumt.edu.cn

Keywords:

Intersected fracture
shear displacement
roughness
channeling flow

Abstract:

This study presents a numerical study on the geometrical and hydraulic properties of a three-dimensional intersected fracture model that is a fundamental element involved in complex fracture networks. A series of rough fracture surfaces were generated using the modified successive random additions (SRA) algorithm. Different shear displacements were applied to the fracture to obtain the anisotropic aperture fields that will be further assigned to the two fractures in the intersected fracture model. The flow was calculated using the Reynolds equation with the continuity conditions addressed at intersection part between the two fracture planes. The evolutions of the aperture distributions, flow channels and equivalent permeability were estimated. The simulation results reveal that as the shear displacement and joint roughness coefficient (JRC) increase, the aperture increases anisotropically, which causes significant fluid flow channeling effects. The main flow channels change from being concentrated in one fracture to the other fracture during the shear, accompanied by the change of the flow rate ratios between two flow planes at the inlet/outlet boundary. During the shear the average contact area accounts for approximately 4% to 15% of the fracture planes, and the actual calculated flow area is about 35% to 42% of the fracture planes, which is smaller than the noncontact area. As the shear displacement and JRC increase, the equivalent permeability of the intersected fracture increases. Therefore, the channeling flow should be considered to interpret the fluid flow through the rough fractures even in the simplest fracture networks.

1. Introduction

Modeling fluid flow and solute transport in fractured rock masses continue to be an attractive issue in different fields from civil and petroleum engineering to the development of radioactive waste repositories (Olsson and Brown, 1993; Gentier et al., 1997; Adler and Thovert, 1999; Cai et al., 2017; Lin et al., 2017; Sidiq et al., 2017). For example, the safety assessment of high-level radioactive waste repositories depends on the knowledge of the fluid flow and solute transport in the connected fracture networks (Tsang et al., 2005). The mechanical behaviors and hydraulic properties of rock masses are greatly influenced by the rock fractures including single fractures, fracture intersections and fracture networks (Berkowitz and Adler, 1998; Darcel et al., 2003; Wei and Xia, 2017). Among them, the single fracture and single

fracture intersection are two basic building blocks to study the flow through rock fracture networks (Kosakowski and Berkowitz, 1999; Li et al., 2016).

Fluid that flows through single fractures has been thoroughly investigated using analytical models, laboratory tests and numerical simulations. Yeo et al. (1998) conducted a series of radial and unidirectional flow experiments in single rough fractures and found that the anisotropy ratio decreased from 0.86 to 0.66 as the shear displacement increases, in which the permeability in the direction perpendicular to the shear direction is larger than that parallel to the shear direction. Auradou et al. (2005) quantified the effect of shear displacement on the permeability anisotropy through rough fractures both experimentally and numerically. They concluded that the permeability parallel to the shear direction decreases significantly while the permeability perpendicular to the shear



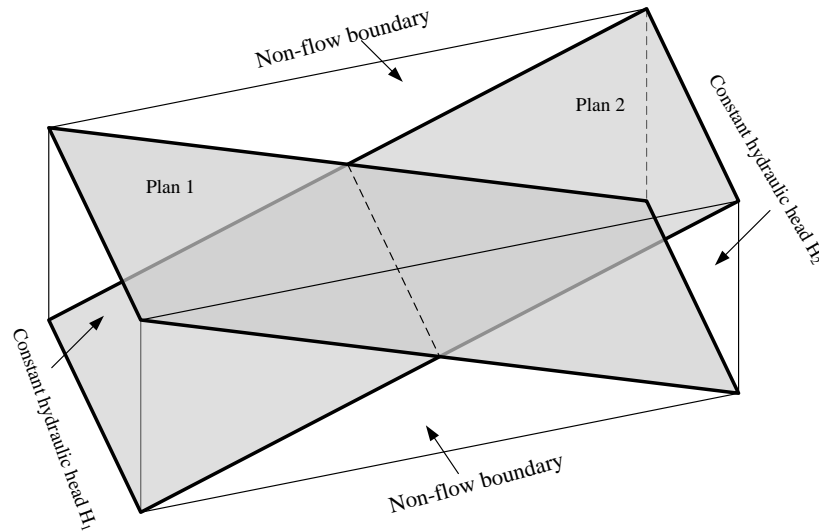


Fig. 1. 3D intersected fracture model and the boundary condition of numerical simulation.

direction increases slightly as the shear displacement increases. Matsuki et al. (2006) generated synthetic fractures of from 0.2 to 12.8 m in size to analyze the size effect on the hydraulic properties of fractures. They concluded that the relation between the hydraulic aperture and the mean aperture is almost independent of fracture size when the shear displacement is less than about 3.1% of the fracture size. Crandall et al. (2010) conducted a series of numerical simulations to examine the relation between the wall-roughness and fluid flow in single rock fracture. The results indicated that fractures with large fractal dimensions were shown to exhibit tortuous flow paths and have a transmissivity 35 times smaller than that of the smoother fractures. Rong et al. (2016) studied the nonlinear flow behavior through single fractures by performing shear flow tests on a series of splitting fractures under different normal stresses. The results showed that the linear and nonlinear coefficients decreased by approximately 1~2 and 1~3 orders of magnitude during shear, respectively.

Many previous studies have focused on the fluid flow and mixing behavior within fracture intersections. Wilson and Witherspoon (1976) conducted a series of laboratory tests to determine the magnitude of laminar flow interference effects at fracture intersections. The results indicated that the interference effects at intersections are negligibly small when the flow is in the laminar regime. Park et al. (2001) analyzed the influences of fracture intersection mixing rules, which contains complete mixing and streamline routing, on simulated solute migration patterns in random fracture networks. They concluded that there is a negligibly small difference between the bulk transport properties calculated using the two mixing rules. Zafarani and Detwiler (2013) proposed a novel probabilistic method to simulate Pe-dependent transport through fracture intersections. The trajectory and travel times of particles passing through the fracture intersection can be accurately represented by the proposed method. The transport modeling and mixing have been studied numerically and analytically. However, the mechanisms responsible for the flow in three-dimensional

fracture intersections are not completely understood, especially the influences of shear-induced fracture aperture anisotropy on the flow redistribution in fracture intersections are rarely analyzed.

Single fractures have traditionally been simplified as parallel plates in which the well-known cubic law relating the volumetric flow with the macroscopic gradient is applied (Witherspoon et al., 1980). Whereas, natural fractures usually display a strong hydraulic complexity coming from the aperture anisotropy induced by the roughness of two fracture walls (Isakov et al., 2001; Auradou et al., 2006; Huang et al., 2017a, 2017b). The hydraulic properties of natural fractures depend on the factors such as surface roughness, aperture distribution and the contact areas between the two opposing faces of the fracture (Baghbanan and Jing, 2008; Rasouli and Hosseinian, 2011; Jafari and Babadagli, 2013). These factors are all closely related with the stress conditions applied on the fractures (Lee and Cho, 2002; Klimczak et al., 2010; Latham et al., 2013; Liu et al., 2018). Normal stress tends to close the fracture thus decreases the permeability of rough fracture, while the shear stress increases the permeability due to the shear-induced dilations.

The purpose of the present paper is to analyze the evolution of aperture field and flow paths that are induced by shear displacement of rough fracture in the 3D fracture intersection. A series of flow simulations were conducted on the model with anisotropic aperture fields to calculate the flow field and the permeability of the model. The evolutions of flow channels and the flow rate ratio between two fracture planes were quantified, and the influences of the fracture roughness on the equivalent permeability were analyzed.

2. Generation of 3D intersected fracture model

The model analyzed in this study consists of two intersecting rough-walled fractures as shown in Fig. 1. The model is $128 \times 50 \times 80$ mm in sizes. For convenience, the two fracture

planes are denoted as fracture plane 1 and fracture plane 2, respectively. Since the fractures are modeled with rough walls, it is critical to assign the fracture surface roughness and calculate the fracture apertures for the two fracture planes in the model.

Based on fractal geometry, the modified successive random additions (SRA) algorithm is used to generate fractional Brownian motion (fBm) for modeling the fracture surface (Liu et al., 2004). If the height of a rough fracture surface is represented by a continuous and single valued function $Z(x, y)$, the stationary increment $[Z(x+hx, y+hy) - Z(x, y)]$ in the fBm framework over the distance $h = \sqrt{h_x^2 + h_y^2}$ displays a Gaussian distribution (Wang et al., 2016). In this study, the two surface walls of the fracture are assumed to be well-matched with the aperture equaling to 0 at the initial state. Then different shear displacements are applied to the fracture to generate aperture fields with anisotropic distributions.

3. Flow calculations

For an incompressible and viscous fluid such as water, its flow is governed by the Navier-Stokes equations that involve a set of nonlinear equations (Neuville et al., 2013; Xie et al., 2015). However, it is usually difficult to solve these equations for fluid flow through the aperture field between two rough fracture walls considering the influence of fracture roughness. Therefore, the flow behavior has been described by using a 2D field by ignoring the tortuosity of the flow across the aperture and assigning the average velocities across the aperture. Correspondingly, the following equation in the X - Y domain can be obtained:

$$\frac{\partial(bu)}{\partial x} + \frac{\partial(bv)}{\partial y} = 0 \quad (1)$$

where b is the aperture, and u and v are the average velocities in the X - and Y - directions, respectively. If the rough fracture aperture field is divided into a set of connected parallel plates with an aperture b at local scale, the following equations can be obtained locally:

$$u = -\frac{b^2}{12\mu} \frac{\partial P}{\partial x} \quad (2)$$

$$v = -\frac{b^2}{12\mu} \frac{\partial P}{\partial y} \quad (3)$$

where P is the pressure and μ is the viscosity of the fluid. By substituting the Eq. (2) and Eq. (3) into Eq. (1), the following equation known as Reynolds equation is obtained to describe the fluid flow through natural rock fractures:

$$\frac{\partial}{\partial x} \left(\frac{b^3}{12\mu} \frac{\partial P}{\partial x} \right) + \frac{\partial}{\partial y} \left(\frac{b^3}{12\mu} \frac{\partial P}{\partial y} \right) = 0 \quad (4)$$

The Reynolds equation is used for the laminar flow in each fracture in the intersected fracture model. For the intersection

between the two fracture surfaces, the following continuity conditions should be satisfied:

$$\begin{cases} h_{k,f} = h_k \\ \sum_{f=1}^2 v_{k,f} \cdot \mathbf{n}_{k,f} = 0 \end{cases} \quad (5)$$

where h_k is the hydraulic head on intersection S_k , $h_{k,f}$ is the trace of the hydraulic head on S_k in fracture plane f , $v_{k,f}$ is the flow velocity through the intersection in fracture plane f and $\mathbf{n}_{k,f}$ is the normal unit vector on the boundary S_k of fracture plane f .

The boundary conditions are the classical permeameter boundary conditions: two fixed hydraulic heads are applied at the inlet and outlet faces (Dirichlet boundary conditions) and other four faces are no flow boundary (Neumann boundary conditions), which can be summarized as:

$$\begin{cases} h = h_1 & \text{on } \Gamma_f \cap \Gamma_{in} \\ h = h_2 & \text{on } \Gamma_f \cap \Gamma_{out} \\ (\nabla h) \cdot \mathbf{n} = 0 & \text{on } \Gamma_f \cap \Gamma_{imp} \end{cases} \quad (6)$$

where Γ_f is the border of fracture f , Γ_{in} and Γ_{out} are the inlet boundary and outlet boundary, respectively, Γ_{imp} is the four impermeable faces and \mathbf{n} is the normal unit vector of the boundary.

The program developed by Huang et al. (2018) is used to solve the steady flow in the intersected fracture model. In this method the flow equation is solved by using the Galerkin's method with the continuity conditions addressed at intersection part between the two fracture planes. The equivalent permeability of the intersected model is estimated using the following equation:

$$Q = A \frac{K}{\mu} \frac{\Delta P}{L} \quad (7)$$

where Q is the total flux through the model that is calculated by summarizing the flow rate of each element on the outlet boundary, A is the cross area of the boundary face, L is the length of the model, and ΔP is the pressure difference between inlet and outlet boundaries.

4. Results and analysis

4.1 Evaluations of aperture distribution and flow path

The surfaces of fractures in the intersected model are generated using the modified SRA algorithm mentioned in the section 2. Then the joint roughness coefficient (JRC) for each fracture surface proposed by Barton and Choubey (1977) is calculated using the following equation:

$$\text{JRC} = 32.2 + 32.47 \log Z_2 \quad (8)$$

where Z_2 is the root mean square of the first derivative of the profile, and can be expressed in the discrete form:

$$Z_2 = \left[\frac{1}{N_t} \sum \left(\frac{z_{i-1} - z_i}{x_{i-1} - x_i} \right)^2 \right]^{1/2} \quad (9)$$

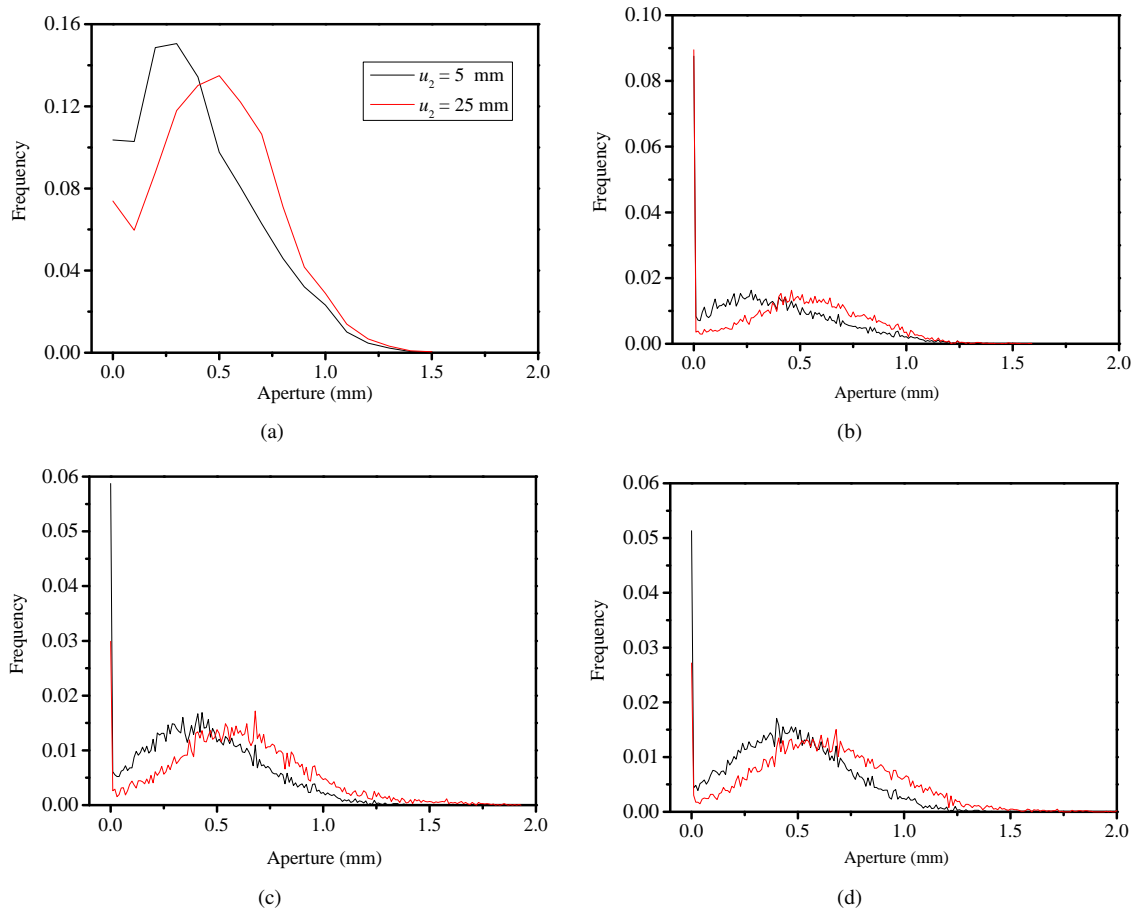


Fig. 2. The frequency histograms of aperture distribution of models with different JRC_2 : (a) $JRC_2 = 6.5$; (b) $JRC_2 = 8.0$; (c) $JRC_2 = 10.3$; (d) $JRC_2 = 14.3$.

where x_i and z_i represent the coordinates of the fracture surface profile, and N_t is the number of sampling points along the length of a fracture. An interval of 0.5 mm for sampling points is selected to calculate the JRC. The mean value of JRC for all the selected profiles is calculated to characterize the roughness of the fracture surface.

For fracture plane 1, one fracture surface with $JRC_1 = 10.26$ is considered, and the apertures calculated under shear displacement $u_1 = 15$ mm are assigned to the fracture plane 1. For fracture plane 2, four different fracture surfaces with $JRC_2 = 6.5, 8.0, 10.3$ and 14.3 , respectively, are considered, and the apertures calculated under shear displacement $u_2 = 5, 10, 15, 20$ and 25 mm, respectively, are assigned to the fracture plane 2. Fig. 2 shows the frequency histograms of aperture distributions of the model under different shear displacements of fracture plane 2 with different JRC_2 . The aperture equaling to 0 indicates the contact between the upper and lower surfaces. The results show that for all cases, the frequency curve shift to the right as u_2 increases. The aperture corresponding to the peak value of the curve increases as the u_2 increases. Comparisons between the curves of four models with different JRC_2 show that the proportion of the larger aperture increases as the JRC_2 increases. This indicates that both the increments of shear displacement and fracture roughness result in the increment of the mean fracture

aperture.

Fig. 3 shows the aperture distribution of the model with different JRC_2 and u_2 . The aperture in fracture plane 1 is maintained with $JRC_1 = 10.26$ and $u_1 = 15$ mm. When $u_2 = 5$ mm, the aperture in fracture plane 2 is small, and there exist a large number of contact points between the fracture surfaces. As u_2 increases from 5 mm to 25 mm, the aperture increases, with some void spaces connected. This phenomenon is more obvious as the JRC_2 increases. As the u_2 and JRC_2 increase, the apertures in fracture plane 2 gradually becomes larger than the apertures in fracture plane 1. The corresponding flow channels are plotted in the Fig. 4, where the main flow paths consist of the elements at which the ratios of local flow rate to the total flow rate (Q_t) are larger than 0.005. The obvious flow channels are distributed in the model, which is caused by the heterogeneous aperture of the fractures. When $JRC_2 = 6.5$ and $u_2 = 5$ mm, the main flow channels exist in fracture plane 1 and there are almost no flow channels in the fracture plane 2. As the u_2 and JRC_2 increase, there start to appear some flow channels in the fracture plane 2. When the $JRC_2 = 14.3$ and $u_2 = 25$ mm, the main flow channels changes from being concentrated in the fracture plane 1 to the fracture plane 2, which indicates that the fracture plane 2 gradually becomes the main flow plane in the model.

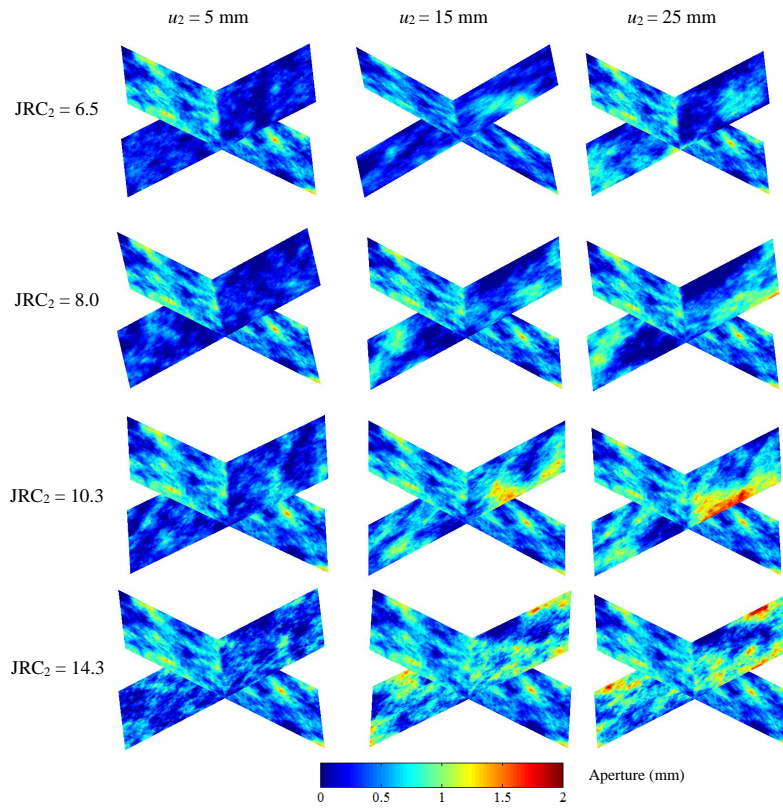


Fig. 3. The aperture distribution of model with different JRC_2 and u_2 .

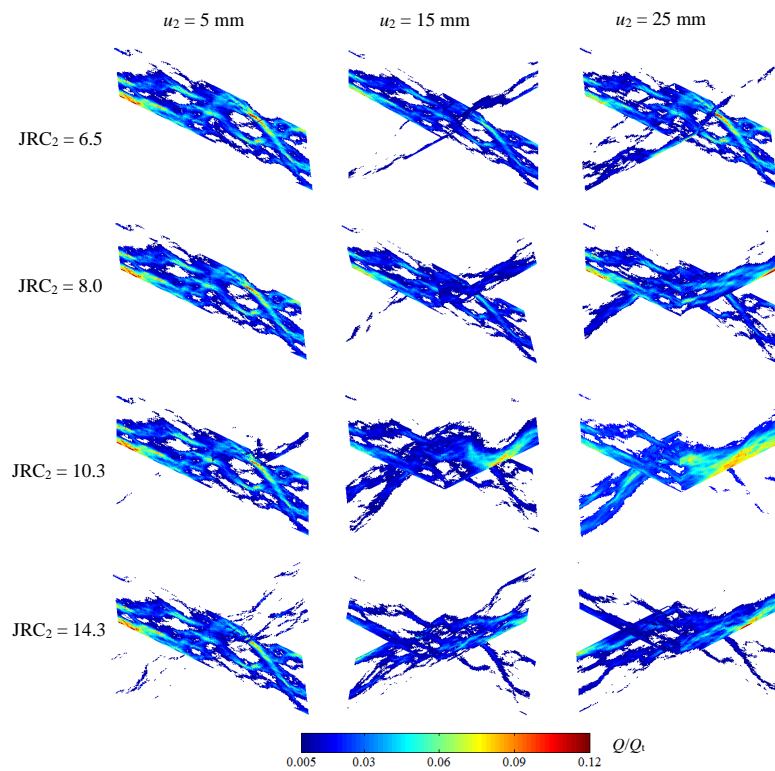


Fig. 4. The main flow paths of models with different JRC_2 and u_2 .

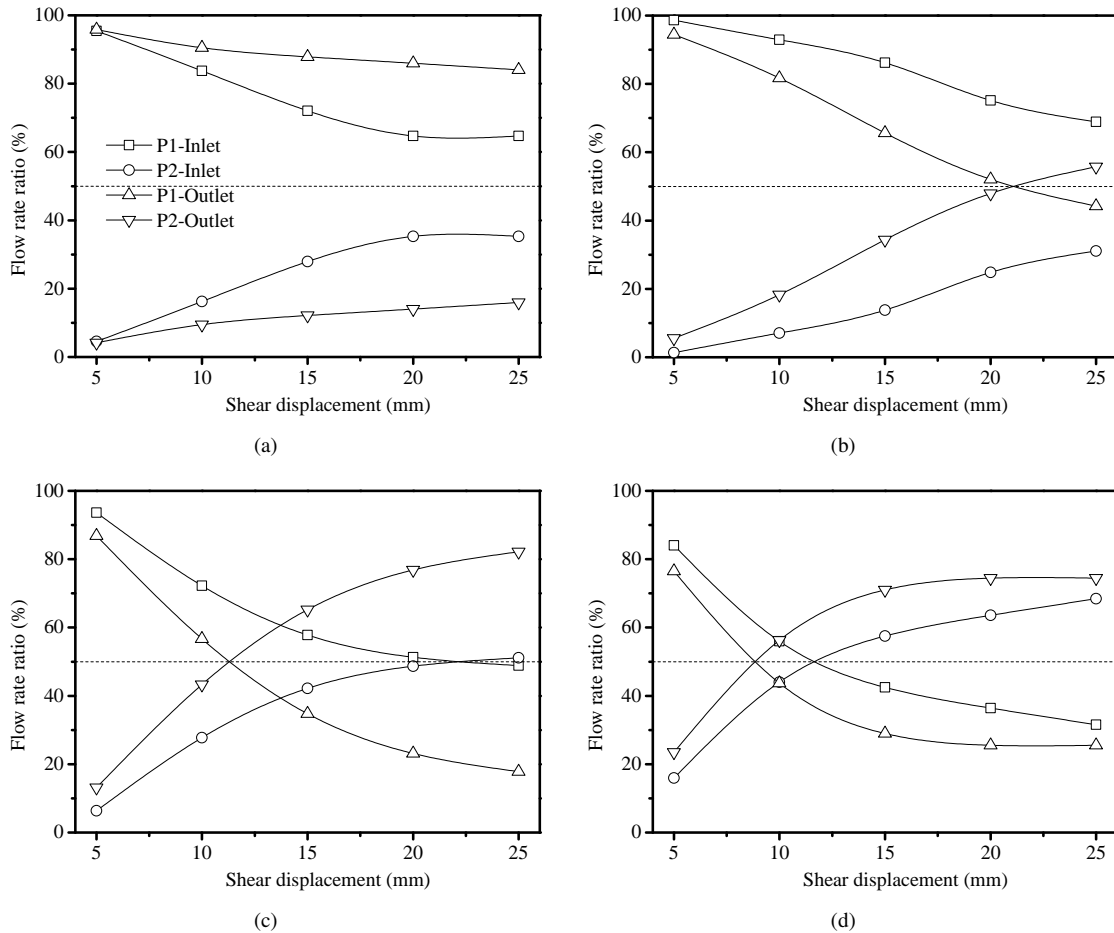


Fig. 5. The flow rate ratio between two fracture planes at inlet and outlet boundaries with different JRC_2 : (a) $JRC_2 = 6.5$; (b) $JRC_2 = 8.0$; (c) $JRC_2 = 10.3$; (d) $JRC_2 = 14.3$.

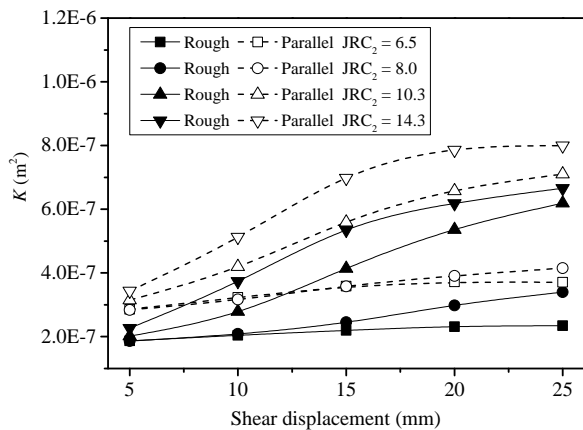


Fig. 7. Comparisons of the equivalent permeability of rough fracture surface model and the equivalent permeability of parallel plate model.

4.2 Flow ratio between two fracture planes

In order to quantify the distribution of flow in the two fracture planes, the flow rate ratio between two fracture planes at inlet and outlet boundaries with different JRC_2 are displayed in Fig. 5. All the curves in the Fig. 5 are symmetrical

along the dash line of 50%. As the shear displacement of fracture plane 2 increases, the flow rate ratio of fracture plane 1 decreases, while the flow rate ratio of fracture plane 2 increases. Comparisons of the curves with different JRC_2 also show the similar tendency. This phenomenon is consistent with the calculated main flow channels in Fig. 4.

The variations of contact areas, flow areas and stagnant areas during shear with different JRC_2 are shown in Fig. 6. The average contact areas account for approximately 4% to 15% of the fracture planes, depending on different u_2 and JRC_2 . The remaining noncontact area of about 96% to 85% of the fracture planes may be the main flow channels through the model. However, due to the roughness of fracture surface, the fluid flows only along some least resistant paths. The calculated flow area is about 35% to 42% of the fracture planes, which is smaller than the noncontact area. The residual area of the fracture planes is the stagnant area.

4.3 Comparison of permeability between rough and parallel fracture model

Natural fractures usually have rough fracture surfaces. The first approximation model for a natural fracture is the parallel plate model that relates the volume flow rate with the cube of

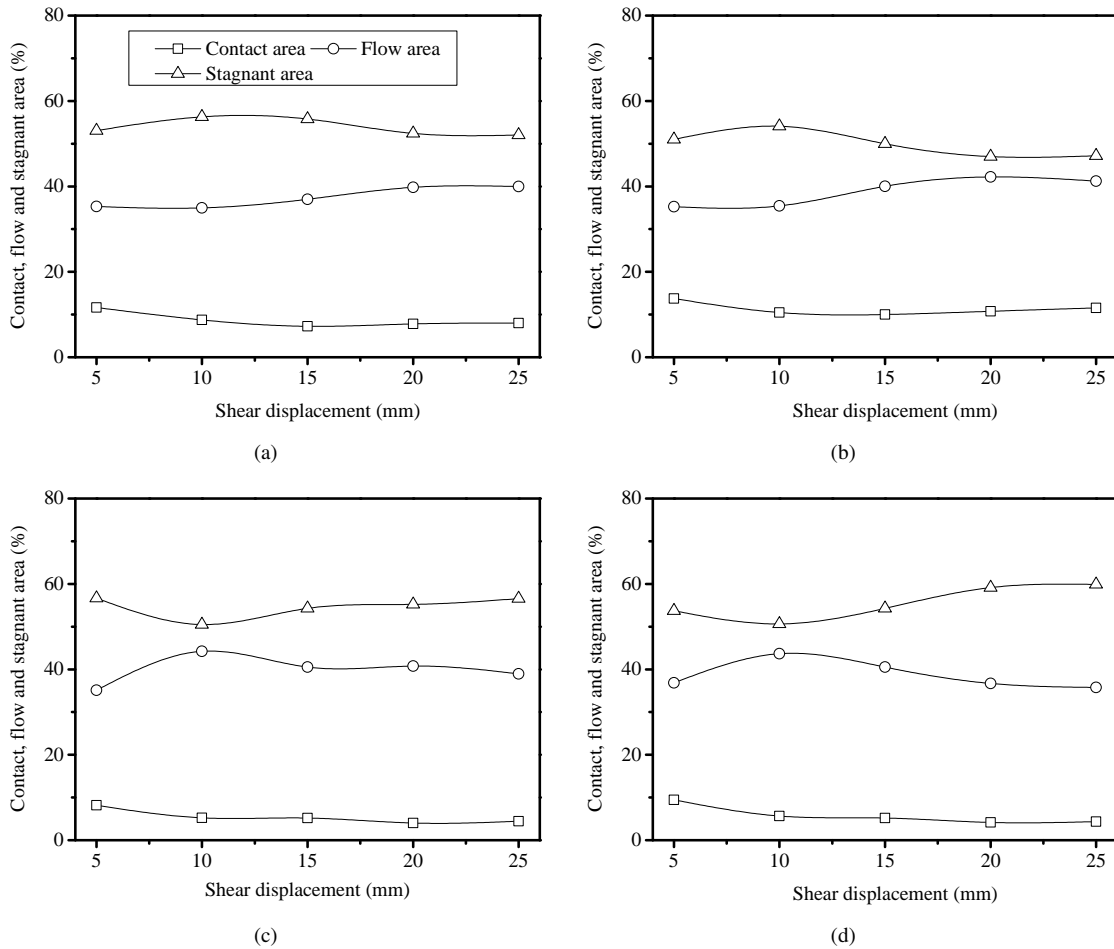


Fig. 6. The variations of contact areas, flow areas and stagnant areas during shear with different JRC_2 : (a) $JRC_2 = 6.5$; (b) $JRC_2 = 8.0$; (c) $JRC_2 = 10.3$; (d) $JRC_2 = 14.3$.

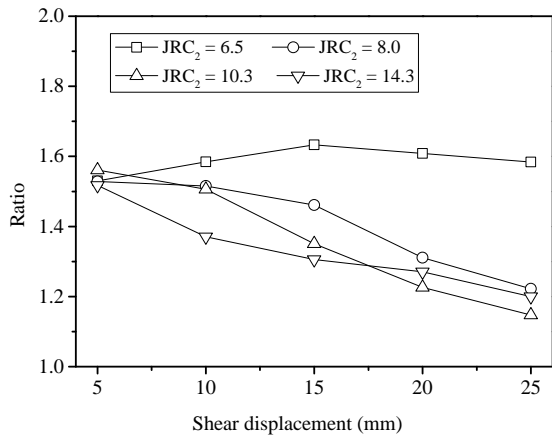


Fig. 8. The ratio of equivalent permeability between parallel plate model and rough fracture surface model.

fracture aperture (Witherspoon et al., 1980). Previous experiments and numerical modeling have demonstrated that there exist deviations between the flow field calculated using a rough fracture surface model and that calculated using a parallel plate model, due to the roughness of the two facing fracture walls (Kim and Inoue, 2003; Li and Jiang, 2013). In order

to analyze this problem for the intersected fracture model, the heterogeneous fractures in the intersected fracture model are replaced by parallel plates that have a distance between the plates equaling to the mean aperture of corresponding fracture in the intersected fracture model. The stagnant area in the rough fractured model is about 50% to 54%, while the stagnant area in the parallel fractured model is 0% because each fracture is assigned to be a same aperture with no contact between the upper and lower surfaces. Then the equivalent permeability for the rough intersected fracture model and the parallel plate model are calculated and compared in Fig. 7. The results show that the equivalent permeability of the two models increases as the shear displacement and JRC_2 increase, with the equivalent permeability of rough fracture surface model always smaller than that of parallel plate model. The ratio of equivalent permeability between parallel plate model and rough fracture surface model is calculated and shown in Fig. 8. The calculated ratios vary between 1.1 and 1.7 and the values fluctuate with the increase of u_2 . This is mainly because of the flow channeling within the fracture plane induced by the aperture heterogeneities. The numerical results may provide important information that when studying the flow characteristic through rough rock fractures, even in the simplest fracture network, the channeling flow should be

considered.

5. Conclusions

In this study, a series of 3D intersected fracture models were generated to study the fracture roughness on their geometrical features and flow behaviors through the models. Rough fracture surfaces with different joint roughness coefficients (JRC) were generated using the modified successive random additions (SRA) algorithm. Different shear displacements were applied on the generated fractures and the corresponding aperture fields were assigned to the fractures in the model. The flow behavior through the model was simulated using the developed numerical code. The evolutions of aperture fields, flow channels, and the flow rate ratio between two fracture planes at the inlet and outlet boundaries were estimated. By comparing the equivalent permeability of rough fractured model with reference to the equivalent permeability of the corresponding model of parallel plate fractures, the influence of fracture roughness on the permeability was analyzed. The following results are obtained:

1. As the shear displacement and JRC of fracture plane 2 increase, the apertures in fracture plane 2 gradually become larger than the apertures in fracture plane 1. At the initial state, the main flow channels exist in the fracture plane 1. As the shear displacement and JRC of fracture plane 2 increase, there exist some flow paths in the fracture plane 2. When the fracture plane 2 changes from $JRC_2 = 6.5$ and $u_2 = 5$ mm to $JRC_2 = 14.3$ and $u_2 = 25$ mm with the fracture plane 1 maintained to be $JRC_1 = 10.26$ and $u_1 = 15$ mm at the initial state, the main flow paths through the model change from mainly existing in fracture plane 1 to fracture plane 2, due to the increase of apertures of fracture plane 2 induced by both the increases of shear displacement and fracture roughness.

2. During the shear, the average contact area accounts for approximately 4% to 15% of the fracture planes, and the actual calculated flow area is about 35% to 42% of the fracture planes, which is smaller than the noncontact area.

3. The flow rate ratio of fracture plane 2 calculated at the inlet/outlet boundary increases with the increasing shear displacement and fracture roughness of fracture plane 2, which indicate the fracture plane 2 gradually becomes the more transmissive fracture than the fracture plane 1.

4. As the shear displacement and JRC of fracture plane 2 increase, the equivalent permeability of the intersected fracture model increases with the equivalent permeability of rough fracture surface model always smaller than that of parallel plate model. In the further, we plan to extend our investigations to involve the influences of mechanical loads on the model, and to study how the normal stress combined with shear stress impacts the hydraulic properties of the intersected fractures.

Acknowledgments

This study has been partially funded by National Natural Science Foundation of China, China (Grant No. 51709260), Natural Science Foundation of Jiangsu Province, China (Grant No. BK20170276), JSPS Grant-in-Aid for Scientific Research,

Japan (Grant No. 17H03506), and JSPS-NSFC Bilateral Joint Research Project, Japan. These supports are gratefully acknowledged.

Open Access This article is distributed under the terms and conditions of the Creative Commons Attribution (CC BY-NC-ND) license, which permits unrestricted use, distribution, and reproduction in any medium, provided the original work is properly cited.

References

- Adler, P.M., Thovert, J.F. Fractures and fracture networks. Springer Science & Business Media, New York, 1999.
- Auradou, H., Drazer, G., Boschan, A., et al. Flow channeling in a single fracture induced by shear displacement. *Geothermics* 2006, 35(5-6): 576-588.
- Auradou, H., Drazer, G., Hulin, J.P., et al. Permeability anisotropy induced by the shear displacement of rough fracture walls. *Water Resour. Res.* 2005, 41(9).
- Baghbanan, A., Jing, L. Stress effects on permeability in a fractured rock mass with correlated fracture length and aperture. *Int. J. Rock Mech. Min.* 2008, 45(8): 1320-1334.
- Berkowitz, B., Adler, P.M. Stereological analysis of fracture network structure in geological formations. *J. Geophys. Res.: Solid Earth* 1998, 103(B7): 15339-15360.
- Cai, J., Wei, W., Hu, X., et al. Fractal characterization of dynamic fracture network extension in porous media. *Fractals* 2017, 25(2): 1750023.
- Crandall, D., Bromhal, G., Karpyn, Z.T. Numerical simulations examining the relationship between wall-roughness and fluid flow in rock fractures. *Int. J. Rock Mech. Min. Sci.* 2010, 47(5): 784-796.
- Darcel, C., Bour, O., Davy, P., et al. Connectivity properties of twodimensional fracture networks with stochastic fractal correlation. *Water Resour. Res.* 2003, 39(10).
- Gentier, S., Lamontagne, E., Archambault, G., et al. Anisotropy of flow in a fracture undergoing shear and its relationship to the direction of shearing and injection pressure. *Int. J. Rock Mech. Min. Sci.* 1997, 34(3-4): 94, e1-94, e12.
- Huang, N., Jiang, Y., Liu, R., et al. A predictive model of permeability for fractal-based rough rock fractures during shear. *Fractals* 2017b, 25(5): 1750051.
- Huang, N., Liu, R., Jiang, Y. Numerical study of the geometrical and hydraulic characteristics of 3D selfaffine rough fractures during shear. *J. Nat. Gas Sci. Eng.* 2017a, 45: 127-142.
- Huang, N., Liu, R., Jiang, Y., et al. Effects of fracture surface roughness and shear displacement on geometrical and hydraulic properties of three-dimensional crossed rock fracture models. *Adv. Water Resour.* 2018, 113: 30-41.
- Isakov, E., Ogilvie, S.R., Taylor, C.W., et al. Fluid flow through rough fractures in rocks I: high resolution aperture determinations. *Earth Planet. Sc. Lett.* 2001, 191(3-4): 267-282.
- Jafari, A., Babadagli, T. Relationship between percolationfractal properties and permeability of 2-D fracture networks.

- Int. J. Rock Mech. Min. 2013, 60: 353-362.
- Kim, H.M., Inoue, J. Analytical approach for anisotropic permeability through a single rough rock joint under shear deformation. *J. Geophys. Resear.* 2003, 108(B8).
- Klimczak, C., Schultz, R.A., Parashar, R., et al. Cubic law with aperture-length correlation: implications for network scale fluid flow. *Hydrogeol. J.* 2010, 18(4): 851-862.
- Kosakowski, G., Berkowitz, B. Flow pattern variability in natural fracture intersections. *Geophys. Resear. Lett.* 1999, 26(12): 1765-1768.
- Latham, J.P., Xiang, J., Belayneh, M., et al. Modelling stress-dependent permeability in fractured rock including effects of propagating and bending fractures. *Int. J. Rock Mech. Min. Sci.* 2013, 57: 100-112.
- Lee, H.S., Cho, T.F. Hydraulic characteristics of rough fractures in linear flow under normal and shear load. *Rock Mech. Rock Eng.* 2002, 35(4): 299-318.
- Li, B., Jiang, Y. Quantitative estimation of fluid flow mechanism in rock fracture taking into account the influences of JRC and Reynolds number. *J. MMIJ* 2013, 129(7): 479-484.
- Li, B., Liu, R., Jiang, Y. Influences of hydraulic gradient, surface roughness, intersecting angle, and scale effect on nonlinear flow behavior at single fracture intersections. *J. Hydrol.* 2016, 538: 440-453.
- Lin, D., Wang, J., Yuan, B., et al. Review on gas flow and recovery in unconventional porous rocks. *Adv. Geo-Energy Res.* 2017, 1(1): 39-53.
- Liu, H.H., Bodvarsson, G.S., Lu, S., et al. A corrected and generalized successive random additions algorithm for simulating fractional Levy motions. *Math. Geology.* 2004, 36(3): 361-378.
- Liu, R., Li, B., Jiang, Y., et al. A numerical approach for assessing effects of shear on equivalent permeability and nonlinear flow characteristics of 2-D fracture networks. *Adv. Water Resour.* 2018, 111: 289-300.
- Matsuki, K., Chida, Y., Sakaguchi, K., et al. Size effect on aperture and permeability of a fracture as estimated in large synthetic fractures. *Int. J. Rock Mech. Min. Sci.* 2006, 43(5): 726-755.
- Neuvillle, A., Flekkøy, E.G., Toussaint, R. Influence of asperities on fluid and thermal flow in a fracture: A coupled lattice Boltzmann study. *J. Geophys. Res.* 2013, 118(7): 3394-3407.
- Olsson, W.A., Brown, S.R. Hydromechanical response of a fracture undergoing compression and shear. *Int. J. Rock Mech. Min. Sci.* 1993, 30(7): 845-851.
- Park, Y.J., Dreuzy, J.R., Lee, K.K., et al. Transport and intersection mixing in random fracture networks with power law length distributions. *Water Resour. Res.* 2001, 37(10): 2493-2501.
- Rasouli, V., Hosseini, A. Correlations developed for estimation of hydraulic parameters of rough fractures through the simulation of JRC flow channels. *Rock Mech. Rock Eng.* 2011, 44(4): 447-461.
- Rong, G., Yang, J., Cheng, L., et al. Laboratory investigation of nonlinear flow characteristics in rough fractures during shear process. *J. Hydrol.* 2016, 541: 1385-1394.
- Sidiq, H., Amin, R., Kennaird, T. The study of relative permeability and residual gas saturation at high pressures and high temperatures. *Adv. Geo-Energy Res.* 2017, 1(1): 64-68.
- Tsang, C.F., Bernier, F., Davies, C. Geohydromechanical processes in the Excavation Damaged Zone in crystalline rock, rock salt, and indurated and plastic clays-in the context of radioactive waste disposal. *Int. J. Rock Mech. Min. Sci.* 2005, 42(1): 109-125.
- Wang, M., Chen, Y.F., Ma, G.W., et al. Influence of surface roughness on nonlinear flow behaviors in 3D self-affine rough fractures: Lattice Boltzmann simulations. *Adv. Water Resour.* 2016, 96: 373-388.
- Wei, W., Xia, Y. Geometrical, fractal and hydraulic properties of fractured reservoirs: A mini-review. *Adv. Geo-energy Res.* 2017, 1(1): 31-38.
- Wilson, C.R., Witherspoon, P.A. Flow interference effects at fracture intersections. *Water Resour. Res.* 1976, 12(1): 102-104.
- Witherspoon, P.A., Wang, J.S.Y., Iwai, K., et al. Validity of cubic law for fluid flow in a deformable rock fracture. *Water Resour. Res.* 1980, 16(6): 1016-1024.
- Xie, L.Z., Gao, C., Ren, L., et al. Numerical investigation of geometrical and hydraulic properties in a single rock fracture during shear displacement with the Navier-Stokes equations. *Environ. Earth Sci.* 2015, 73(11): 7061-7074.
- Zafarani, A., Detwiler, R.L. An efficient time-domain approach for simulating Pe-dependent transport through fracture intersections. *Adv. Water Resour.* 2013, 53: 198-207.